LARGE-SCALE BIOLOGY ARTICLE

Tissue- and Cell-Type Specific Transcriptome Profiling of Expanding Tomato Fruit Provides Insights into Metabolic and Regulatory Specialization and Cuticle Formation [W][OA]

Antonio J. Matas,[a] Trevor H. Yeats,[a] Gregory J. Buda,[a] Yi Zheng,[b] Subhasish Chatterjee,[c] Takayuki Tohge,[d] Lalit Ponnala,[e] Avital Adato,[f] Asaph Aharoni,[f] Ruth Stark,[c] Alisdair R. Fernie,[d] Zhangjun Fei,[b,g] James J. Giovannoni,[b,g] and Jocelyn K.C. Rose[a,1]

[a] Department of Plant Biology, Cornell University, Ithaca, New York 14853
[b] Boyce Thompson Institute for Plant Research, Cornell University, Ithaca, New York 14853
[c] Department of Chemistry, City College of New York, City University of New York Graduate Center and Institute for Macromolecular Assemblies, New York, New York 10031
[d] Max-Planck-Institut für Molekulare Pflanzenphysiologie, 14476 Potsdam-Golm, Germany
[e] Computational Biology Service Unit, Cornell University, Ithaca, New York 14853
[f] Department of Plant Sciences, Weizmann Institute of Science, Rehovot 76100, Israel
[g] U.S. Department of Agriculture–Agricultural Research Service, Robert W. Holley Center for Agriculture and Health, Cornell University, Ithaca, New York 14853

Tomato (*Solanum lycopersicum*) is the primary model for the study of fleshy fruits, and research in this species has elucidated many aspects of fruit physiology, development, and metabolism. However, most of these studies have involved homogenization of the fruit pericarp, with its many constituent cell types. Here, we describe the coupling of pyrosequencing technology with laser capture microdissection to characterize the transcriptomes of the five principal tissues of the pericarp from tomato fruits (outer and inner epidermal layers, collenchyma, parenchyma, and vascular tissues) at their maximal growth phase. A total of 20,976 high-quality expressed unigenes were identified, of which more than half were ubiquitous in their expression, while others were cell type specific or showed distinct expression patterns in specific tissues. The data provide new insights into the spatial distribution of many classes of regulatory and structural genes, including those involved in energy metabolism, source-sink relationships, secondary metabolite production, cell wall biology, and cuticle biogenesis. Finally, patterns of similar gene expression between tissues led to the characterization of a cuticle on the inner surface of the pericarp, demonstrating the utility of this approach as a platform for biological discovery.

INTRODUCTION

The fleshy fruits of angiosperms have evolved complex physiologies and regulatory mechanisms to promote seed dispersal and are important components of human and animal diets. Much of what is known about fleshy fruit organogenesis, development, and maturation and the molecular bases of organoleptic and nutritional qualities has resulted from studies of tomato (*Solanum lycopersicum*), the principal model for fleshy fruit biology (Giovannoni, 2004; Tanksley, 2004; Paran and van der Knaap, 2007; Seymour et al., 2008; Matas et al., 2009; Klee, 2010).

Research resources for tomato include linkage maps, extensive mapping and breeding germplasm collections (Gur et al., 2004; Bombarely et al., 2011), and a substantial molecular and genomic toolbox (Yano et al., 2006; Bombarely et al., 2011; Fei et al., 2011), including the release and updates of a high-quality genome sequence (http://solgenomics.net). This infrastructure has promoted major advances in the study of fruit molecular biology, physiology, and biochemistry and more recently has laid the foundation for large-scale profiling of tomato fruit transcriptomes (Alba et al., 2004, 2005; Wang et al., 2009; Osorio et al., 2011), proteomes (Faurobert et al., 2007; Yeats et al., 2010; Catalá et al., 2011), and metabolomes (Bino et al., 2005; Carrari and Fernie, 2006; Carrari et al., 2006; Nashilevitz et al., 2010). Such "omics" scale analyses are providing insights into the intricate networks of structural and regulatory genes that mediate many aspects of fruit development.

However, a limitation of most such studies of tomato fruit biology to date, whether examining specific phenomena or taking a nontargeted "omics" approach, is that they have mostly

used total homogenized tomato fruit pericarp (flesh), thereby ignoring spatial variation in transcript, protein, or metabolite accumulation in the different constituent tissue and cell types. Consequently, many layers of information are obscured or missing entirely. Valuable spatial data are lost, and lower abundance cellular components that are present only in certain cell types are thereby diluted below the level of detection, particularly when those cell or tissue types represent a disproportionately small portion of the organ.

Tomato fruits comprise multiple complex tissues (Figure 1A), as well as seeds, some of which undergo major changes in structure and morphology during development and ripening. Some studies of gene expression have reduced the sample complexity by targeting specific parts of the organ, such as fruit peels (Mintz-Oron et al., 2008; Zhang et al., 2008). However, while this strategy has provided a degree of spatial resolution, plant material isolated by relatively crude peeling inevitably contains varying proportions of multiple pericarp cell types. A more precise alternative for isolating specific cell or tissue types is laser capture microdissection (LCM; also termed laser microdissection), which has been applied to profile gene expression in a range of vegetative plant tissues or cell types, including abscission zones, vascular bundles, parenchyma, incipient leaves, root tissues, and meristems (Cai and Lashbrook, 2008; Nelson et al., 2008; Agustí et al., 2009; Brooks et al., 2009; Jiao et al., 2009). Such studies of low abundance tissues have resulted in the identification of a relatively large number of previously unannotated genes, demonstrating the value of LCM as a tool for gene discovery. Moreover, the functions of many genes may be inferred, or at least assigned to a set of functional categories, based on the patterns of tissue or cell type–related expression.

The aim of this study was to determine the extent to which tissue-specific transcript profiling could similarly provide insights into fruit physiology and compartmentation of biochemical pathways and structures. The potential of this approach was previously suggested through a pilot analysis in which we monitored transcript expression in LCM-isolated epidermal and subepidermal layers of citrus fruits (Matas et al., 2010), revealing considerable spatial variation. Here, we describe the simultaneous transcriptome profiling of all five major cell types/tissues of the tomato fruit pericarp (Figure 1), including the outer epidermis (a single cell layer), collenchyma (approximately three to five cell layers in the Ailsa Craig cultivar used in this analysis), parenchyma (~15 to 20 cell layers), vascular tissue (xylem, phloem, and affiliated cells), and inner epidermis (a single cell layer). These cell types show clear evidence of functional and metabolic specialization, such as the presence of a thick hydrophobic cuticle coating the outer epidermis, and spatially distinct, but adjacent, tissues that function as either sources of energy (chloroplast rich collenchyma cells) or energy sinks (parenchyma cells, where starch granules accumulate). Such obvious morphological features hint at extensive and complex tissue-related variation in gene expression. Furthermore, we targeted growing fruits at their maximum rate of expansion, when carbohydrate metabolism and cell wall and cuticle biosynthesis are prominent features. Our presumption was that this would further enhance differences in expression between tissue and
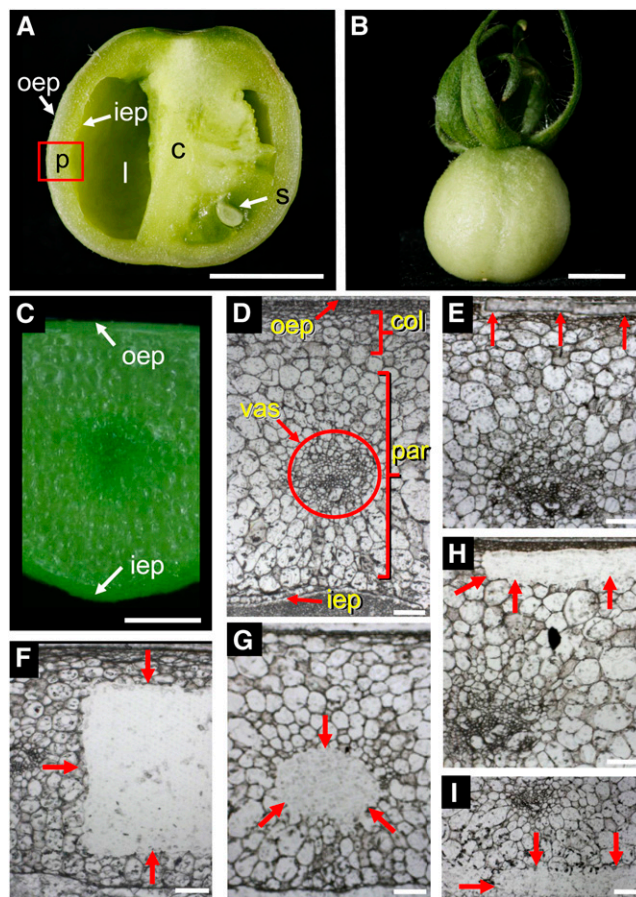

Figure 1. LCM of Tomato (cv Ailsa Craig) Fruit Pericarp Tissues.

(A) Bisected tomato fruit showing the pericarp (p), an empty locule (l), columella (c), seed (s), outer epidermis (oep), and inner epidermis (iep) of the pericarp. Box indicates the portion of pericarp collected for LCM. Bar = 5 mm.
(B) Fruit at 10 DPA. Bar = 5 mm.
(C) Detail of the pericarp used for LCM. Bar = 1 mm.
(D) to **(I)** Cryosection of the tomato fruit pericarp showing the outer epidermis (oep), collenchyma (col), vascular bundle (vas), parenchyma (par), and inner epidermis (iep) of the pericarp **(D)** after LCM of the areas highlighted with arrows of the outer epidermis **(E)**, pericarp **(F)**, vascular bundle **(G)**, collenchyma **(H)**, and inner epidermis **(I)**. Bars = 100 μm.

cell types, thus revealing genes associated with these activities.

To obtain deep transcriptome coverage, we used 454 pyrosequencing, rather than the microarray approach that was used in our preliminary study of citrus fruit (Matas et al., 2010). We present data confirming that coupling of LCM with new sequencing technologies can provide numerous insights into fruit tissue–specific regulatory and metabolic pathways. We also describe the identification and analysis of a cuticle, the existence of which was initially suggested to us as a result of the LCM expression profiling, demonstrating the value of this approach as a platform for biological discovery.

RESULTS

Laser Microdissection and RNA-Seq Analysis of Tomato Fruit Pericarp Tissues

Several techniques were tested to optimize the preparation of tomato fruit 10 d postanthesis (DPA; Figure 1B) pericarp samples for sectioning and laser microdissection, including fixation with acetone or ethanol:acetic acid, paraffin embedding and sectioning, or cryosectioning. A fixation treatment with ethanol:acetic acid, followed by sucrose cryoprotection and cryosectioning, resulted in the best preservation of tissue morphology (Figures 1C and 1D) and allowed clear identification of the five major pericarp tissues: outer epidermis, collenchyma, parenchyma, vasculature, and inner epidermis (Figures 1D to 1I). The tissues were isolated by LCM; RNA was extracted from ~400 cells per tissue prior to mRNA selection and two rounds of amplification. This protocol resulted in between 35 and 70 μg of amplified RNA per tissue, which was pyrosequenced using the 454 FLX platform, yielding a total of 1,061,255 raw reads (data archived at the National Center for Biotechnology Information [NCBI] Sequence Read Archive under accession number SRP004923). A total of 20,976 high-quality unigenes (those with at least five consistently overlapping reads) were then defined, following processing to remove low-quality regions and adaptor sequences and sequence assembly (see Supplemental Table 1 online). Of these, ~88% (18,407) could be assigned an annotation based on database sequence homology. The annotated list of these unigenes, together with average length, number of raw reads that were used for each unigene assembly, and normalized digital gene expression, are provided in Supplemental Data Set 1 online.

As a first step, we examined the tissue specificity of the unigenes. Approximately 57% were expressed in all five tissues, whereas only 3% (624) were tissue specific, and the rest were distributed among different tissue combinations (Figure 2A). Of the 624 cell/tissue-specific unigenes, collenchyma and parenchyma had the lowest number (~6 and 4%, respectively) and the outer epidermis (35%) and vascular bundle (46%) the highest. Of the nonadjacent tissues, those sharing the greatest number of overlapping expressed genes are the outer and inner epidermal tissues. Principal component analysis supported these results, revealing a close grouping of collenchyma, parenchyma, and inner epidermis (Figure 2B), while the vascular tissue shows clear variance and the outer epidermis the most different of the five tissues, with PC1 and PC2 explaining >83% of the variance.

In addition to this qualitative assessment, quantitative differences were determined by pairwise comparisons of transcript abundance for each unigene among the different pericarp tissues. A total of 43% (8967) of the 20,976 high quality unigenes had significantly different transcript levels (P < 0.05) in at least one of the six combinations (each tissue compared with parenchyma as well as outer epidermis:collenchyma and outer epidermis:inner epidermis; http://ted.bti.cornell.edu/cgi-bin/TFGD/digital/home.cgi). Of these pairwise comparisons, the combination with the greatest number of unigenes showing significant differences in transcript levels from each other was outer epidermis versus collenchyma, with 1875 and 1805, respectively.
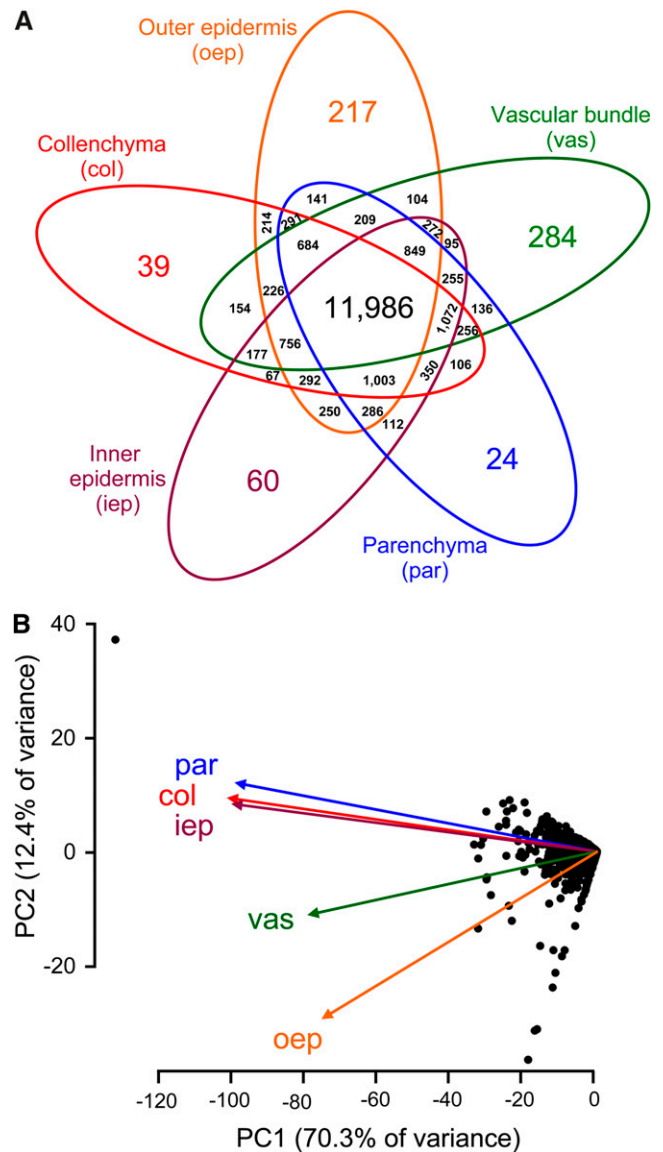

Figure 2. Tomato Fruit Pericarp Tissue-Related Transcript Expression Profiles.

(A) Venn diagram showing unigene expression distribution among the five pericarp tissues.
(B) Principal component analysis of the tissue-associated transcriptome.

Similarly, vascular tissue and parenchyma showed large numbers of differentially expressed transcripts, with 2183 and 1445, respectively. Conversely, the collenchyma and parenchyma transcript comparison showed the lowest numbers, with 666 and 532, respectively.

An analysis of Gene Ontology (GO) terms associated with each of the tissue predominant transcript populations provided further evidence of pericarp tissue functional specialization (see Supplemental Figure 1 online). For example, both the outer epidermis and vascular tissue had significantly more transcripts associated

with transport and responses to stress, while the outer and inner epidermal tissues showed an increased frequency of transcripts associated with lipid metabolic processes. Given the known functions of these tissues, these distributions might be predicted; however, other term enrichments are more difficult to explain, such as the preponderance of the term "protein binding" associated with vascular tissues.

A Hierarchical Cluster Analysis Reveals Tissue Specificities and Associations between Tissues

All the high-quality unigenes were used in a hierarchical cluster analysis of transcript abundance across the five tissue types, which revealed ten main clusters (Figure 3A; see column H in Supplemental Data Set 1 online). Of these, only two (II.B with 3985 unigenes in the outer epidermis and II.A.2 with 3832 unigenes in the vascular tissue) corresponded to a set of genes that are predominantly expressed in a single tissue. These two tissues were also determined by principal component analysis to show the greatest qualitative variance in transcript expression (Figure 2B). Other clusters represented patterns of transcript accumulation involving different tissue combinations. Some of these clusters corresponded to adjacent pericarp tissues, such as cluster I.A.1.a (Figure 3B), with genes highly expressed in the outer tissues (outer epidermis and collenchyma), or its counterpart, cluster I.B.1, corresponding to transcripts that are particularly abundant in the inner tissues (vascular, parenchyma, and inner epidermis). In some cases, the clusters contained genes whose annotation clearly suggests a similar function or association with a related physiological process. For example, cluster II.A.1 (Figure 3A) includes genes that are predominantly expressed in outer epidermis and vascular bundle and that, from their annotations, could be associated with water stress responses. Likewise, cluster I.B.2.a (Figure 3B) corresponds to genes that are preferentially expressed in outer and inner epidermal tissues, many of which can be functionally related to cuticle metabolism and defense.

In a separate analysis, we considered only the unigenes that showed significantly different transcript abundance levels in the pairwise comparisons (the analysis in Figure 3 incorporated all the unigenes). Analysis of this subset (see Supplemental Data Set 2 online) combined the spatial pattern distribution shown in Figure 3 with transcript abundance information (http://ted.bti.cornell.edu/cgi-bin/TFGD/digital/home.cgi), providing important support for the correspondence between the clusters and tissue associations. Thus, collenchyma-predominant genes were distributed among clusters I.A.1.a, I.A.1.b.1, and I.A.1.b.2, which also contain genes that are expressed abundantly in the outer epidermis. Parenchyma-predominant genes were mostly present in cluster I.A.2 but were also present in clusters I.B.1 and I.B.2.b, both of which also contain many inner epidermis abundant genes. Another substantial subset of the inner epidermis–related genes are found in cluster I.B.2.a, together with genes that are mostly expressed in the outer epidermis. Cluster II.A.1 contained genes that were significantly abundant in both vascular and outer epidermis, while clusters II.A.2 and II.B were almost exclusively populated with vascular and outer epidermis significantly abundant genes, respectively.

Differential Expression of Transcription Factors among Fruit Tissue Types

A total of 821 annotated transcription factors showed differential expression among the various pericarp tissues (see Supplemental Data Set 3 online), including members of the AP2/ERF, MADS, MYB, NAC, and WRKY families. Vascular tissues contained the greatest number of tissue-specific transcription factors (eight), while none were detected in parenchyma (see Supplemental Figure 2A online). Some of the most abundant differentially expressed transcription factors, such as those annotated as hypothetical proteins, could not be assigned to known families, with additional representation among auxin and ethylene response regulators, as well as several MADS box and NAC domain protein encoding genes. The most abundantly expressed transcription factor that showed differential expression between tissues is a member of the mini zinc finger family (TU056956), with more than 600 normalized reads, which is twice the number of the next most abundant (BTF3-like transcription factor, TU043758). However, the most differentially expressed transcription factor overall was *cutin deficient2* (TU043252), which is 80-fold more abundant in the outer epidermis than in vasculature tissues and is also expressed at high levels in the inner epidermis. Some transcription factors with previously reported roles in fruit development were identified, such as TAGL1 (TU027535), which is among the most abundant MADS box proteins expressed in the tissues analyzed. TAGL1 has been associated with early development of carpel fleshiness (Itkin et al., 2009; Vrebalov et al., 2009; Pan et al., 2010), but while previous reports of TAGL1 expression and function measured transcript levels in whole pericarp tissues, here, we show that TAGL1 is expressed at high levels in all five assayed carpel tissues and, thus, likely promotes carpel expansion across the spectrum of carpel tissues. Other transcription factors that can be linked with specific metabolic processes also showed distinct patterns of spatial expression. For example, MYB proteins have been associated with accumulation of anthocyanins and related phenylpropanoids, and although a number of putative MYB genes show differential expression in the tissues analyzed, only one shows predominance in the outer and inner epidermal tissues (TU024673).

Differential Expression of Energy Metabolism–Associated Genes

Many studies have examined carbohydrate- and energy-related metabolic pathways in tomato fruit at the level of transcripts (Kolotilin et al., 2007; Kahlau and Bock, 2008; Karlova et al., 2011), proteins (Vega-Garcia et al., 2010), enzyme activities (Kanai et al., 2007; Steinhauser et al., 2010), or metabolites (Shahbazi et al., 2007; Karlova et al., 2011). However, all these analyses involved homogenized fruits with no consideration of spatial variation among tissue types. We therefore evaluated the fruit tissue–related distribution and relative transcript levels of genes associated with energy metabolism, including those annotated as contributing to photosynthesis and photorespiration, focusing on gene families in which multiple members were differentially expressed.
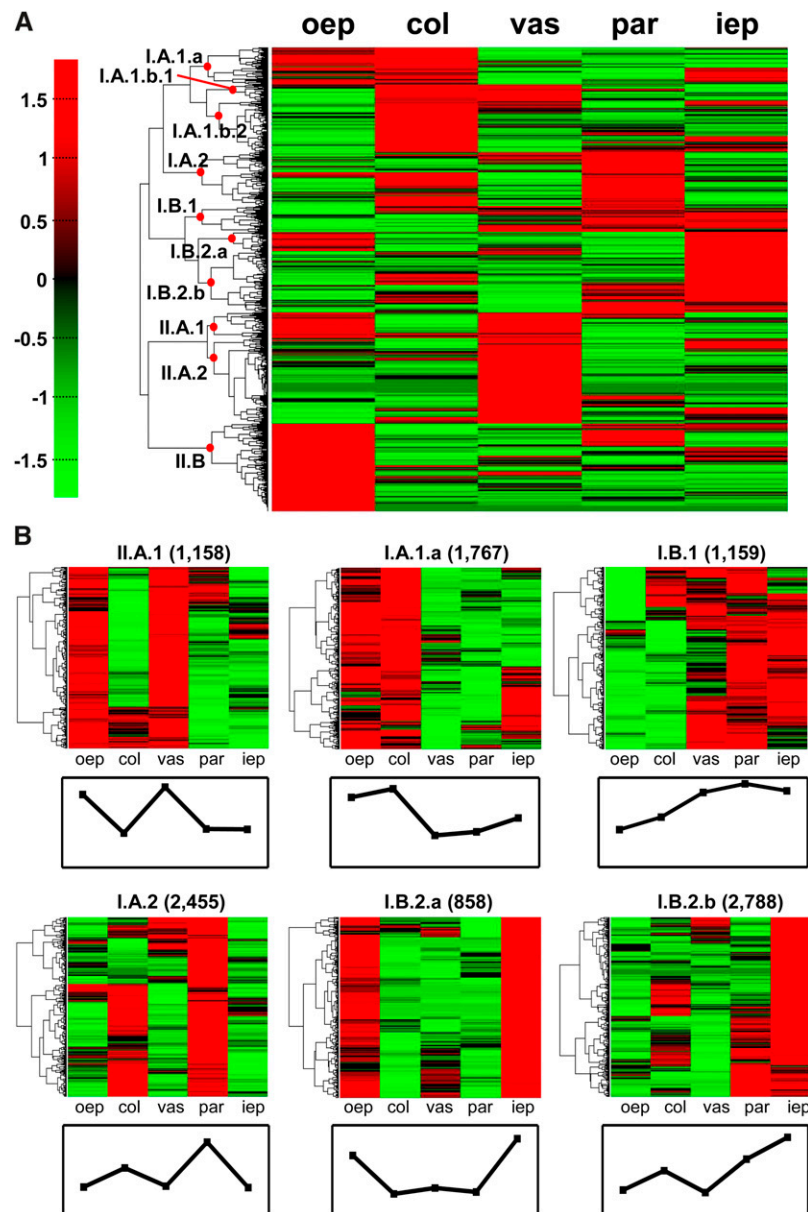
Figure 3. Hierarchical Cluster Analysis of Transcript Expression Profiles in Five Tomato Pericarp Tissues.

(A) Cluster analysis was performed using the transcript data from collenchyma (col), vascular bundle (vas), parenchyma (par), and outer epidermis (oep) and inner epidermis of the pericarp (iep). Clusters of interest are indicated with a red dot at the node and cluster number. Red and green colors represent pairwise distances among transcript above or below, respectively, the mean (black) across all five tissues.
(B) Magnified regions of clusters of interest, based on certain patterns of tissue expression, showing the cluster number, with the number of associated unigenes in parentheses.

A total of 103 unigenes putatively corresponding to the Calvin-Benson cycle were identified (Figure 4). Most were expressed at considerably lower levels in the outer epidermis than the parenchyma but at higher levels in the collenchyma than the parenchyma. However, this was not always the case: ribulose-1,5-bis-phosphate carboxylase/oxygenase (no unigene is present at higher levels [>2.0], five at lower levels [<0.5], and one at no expression in collenchyma) and fructose-bisphosphate al-dolase (nine unigenes are present at higher levels [>2.0], seven at lower levels [<0.5], and three at no expression in collenchyma) exhibited mixed patterns. It is important to note that not all of these genes may be associated with photosynthesis, since several of the fructose-bisphosphate aldolases are likely to be localized in the cytosol. The comparison between vascular tissues and parenchyma showed a clearer trend, with the majority (27 of the 89 unigenes detected) expressed at lower levels
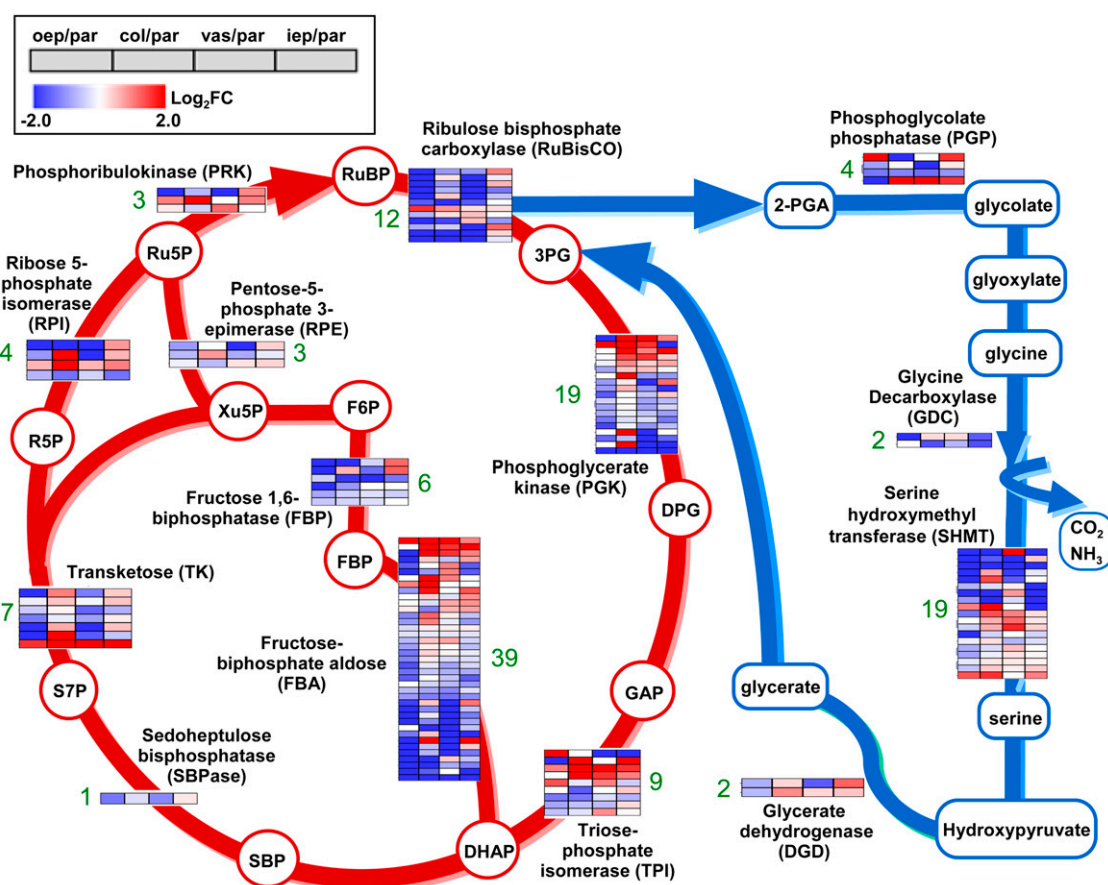
Figure 4. Relative Expression in Different Pericarp Tissues of Transcripts Associated with the Calvin-Benson Cycle and Photorespiration.

Unigenes identified in this study associated with 14 enzymatic gene families that are components of the Calvin-Benson cycle and photorespiration were placed on their respective pathways using Plant MetGenMAP for tomato (http://bioinfo.bti.cornell.edu/cgi-bin/MetGenMAP/home.cgi) and MetaCyc (http://metacyc.org). The inset shows the color coding for the logarithmic fold change (log$_2$FC) of gene expression of respective comparisons (log$_2$FC > 2.0 is in red; log$_2$FC > −2.0 is in blue) as well as the representation of each pairwise tissue comparison: outer epidermis (oep), collenchyma (col), vascular bundle (vas), parenchyma (par), and inner epidermis (iep) of the pericarp. The numbers of unigenes corresponding to each enzyme class are shown in green. Boxes in the vertical axis showing gene expressions of each gene set were clustered by MeV HCA (Howe et al., 2010) using Euclidean distance as the measurement of similarity. 2PGA, 3-phosphoglycolate; 3PG, 3-phospho-D-glycerate; DHAP, dihydroxyacetone phosphate; DPG, 1,3-diphosphsteglycerate; F6P, D-fructose-6-phosphate; FBP, fructose-1,6-biphosphate; GAP, D-glyceraldehyde-3-phosphate; R5P, D-ribose-5-phosphate; Ru5P, D-ribulose-5-phosphate; RuBP, D-ribulose-1,5-biphosphate; S7P, D-sedoheptulose-7-phosphate; SBP, D-sedoheptulose-1,7-biphosphate; Xu5P, D-xylulose-5-phosphate.

in the vascular tissue. The comparison of inner epidermis and parenchyma revealed a similar mixed pattern with 19 of the 97 genes associated with the Calvin-Benson cycle expressed at higher levels in the inner epidermis and 18 at lower levels. Genes associated with the photorespiratory pathway also exhibited differential expression across the pericarp tissues (Figure 4), which is congruent with the intimate association with ribulose-1,5-bis-phosphate carboxylase/oxygenase via the oxygenase reaction and the carboxylase reaction, which is central to the Calvin-Benson cycle (Bauwe et al., 2010). There were also spatial variations in the expression of unigenes encoding phosphoglycolate phosphatase (four unigenes: TU123333, TU045988, TU055311, and TU122763), Gly decarboxylase (two unigenes: TU036022 and TU127574), Ser hydroxymethyltrans-ferase (SHMT; 21 unigenes), and glycerate dehydrogenase (two unigenes; TU049449 and TU054074). As was observed for photosynthesis, the outer epidermis showed reduced levels of expression of glycerate dehydrogenase compared with collenchyma, parenchyma, or inner epidermis, while collenchyma and inner epidermis both had higher expression than the parenchyma. Most of the genes encoding SHMT displayed a similar expression pattern; however, this was not always the case, possibly reflecting the fact that SHMTs are thought to exhibit a very broad range of functions and may participate in processes other than photorespiration (Maurino and Peterhansel, 2010; Zhang et al., 2010). Unigenes associ-ated with starch biosynthesis were consistently expressed at higher levels in the collenchyma than the outer epidermis,

although no such clear patterns were seen in the other tissue comparisons.

Many other changes that are indicative of spatial variation in metabolism were also apparent when analyzing the data on a gene-by-gene basis. For example, the outer epidermis had generally higher levels of transcripts associated with sugar, organic acid, and nitrate transporters and lower levels of most of the enzymes of the tricarboxylic acid (TCA) cycle than other tissues. Conversely, the outer epidermis had lower expression of members of the mitochondrial carrier family protein and most enzymes of the TCA cycle, as well as the electron transfer flavo-protein complex, which is generally upregulated in the absence of light (Ishizaki et al., 2005). Transcripts of secondary metabolite–related genes in the flavonol biosynthesis pathway, including chalcone synthase (nine unigenes), flavanone 3-hydoxylase (four unigenes), flavonol synthase (seven unigenes), and flavonoid glycosyltransferase (GT; TU120090), were substantially greater in the outer epidermis (see Supplemental Figure 3 online). By contrast, genes associated with biosynthesis of carotenoids and alkaloids did not show consistent spatial variation in expression levels in each pairwise comparison.

Differences in Cell Wall Biosynthesis and Disassembly

Fruit ontogeny provides an excellent opportunity to study cell wall dynamics, including assembly, restructuring, and disassembly. There are many examples in the literature describing structural and compositional changes in wall polymers during tomato fruit development, enzyme activities that correlate with wall modification, and the expression of corresponding gene families (Rose et al., 2003; Brummell, 2006; Vicente et al., 2007; Matas et al., 2009). However, many fundamental questions remain entirely unresolved, largely because such studies have used homogenized pericarp tissues. For example, there is some indication that wall structure is likely to vary considerably between pericarp layers (Huysamer et al., 1997), yet little is known about spatial variation in wall metabolism. To investigate potential differences in the cell wall metabolism of the different pericarp tissues, we used the tomato unigene annotations to identify 253 GTs and 293 glycosyl hydrolases (GHs) related to cell wall biogenesis and disassembly, respectively. Approximately 59% of GTs and 55% of GHs were present in all tissues with different levels of expression (see Supplemental Figures 4A and 4B online, respectively). Few genes were tissue specific, but of those, most were expressed only in the vascular tissues (four GTs and four GHs), and the other genes were distributed among the other tissues. It was notable that the largest groups comprised GTs or GHs that were expressed in all tissues except the vascular tissue or the outer epidermis, the two tissues that also showed the greatest variation in overall unigene expression (Figure 2B).

We also found an uneven distribution of predicted GHs and GTs among the unigene clusters shown in Figure 3 that indicate patterns of tissue associated transcript abundance (Figure 5). The proportion of GHs is higher in clusters that include epidermis or vascular tissue predominant expression, such as clusters I.B.2.a (inner and outer epidermis), I.B.2.b (inner epidermis), II.B (outer epidermis), and II.A.2 (vascular tissues). GTs showed a different pattern and tended to be associated with clusters
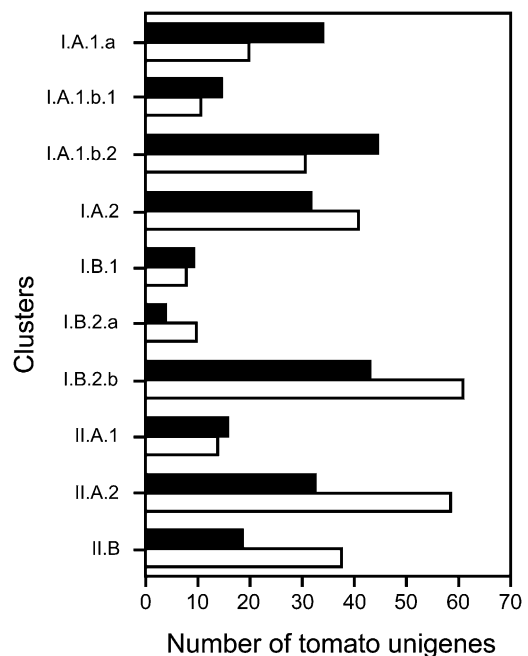

Figure 5. Cluster Distribution of Unigenes Associated with Cell Wall Biosynthesis and Disassembly.

Distribution of unigenes corresponding to cell wall GTs (black bars) and GHs (white bars) among the predicted hierarchical clusters shown in Figure 3.

related to collenchyma predominant unigenes (1.A.1.a, 1.A.1.b.1, and 1.A.1.b.).

Genes Associated with the Tomato Fruit Cuticle

One of the most obvious structural features of the tomato fruit pericarp is the thick waxy cuticle that coats the outer epidermal cells and that often ramifies in the apoplast of some of the underlying cell layers in mature fruit (Buda et al., 2009). The cuticle is believed to be synthesized specifically by the outer epidermal tissue and so it would be reasonable to assume that the genes associated with cuticle biosynthesis, deposition, and restructuring would be particularly abundant, if not specifically expressed, in this tissue. Moreover, it would be likely that the expression levels of genes associated with cuticle formation and function would be high at the 10-DPA stage of fruit development used in this study since this represents the most rapidly expanding stage and, accordingly, a phase of pronounced cuticle biosynthesis (Yeats et al., 2010). We therefore investigated the expression of genes whose annotation suggested a potential association with lipid or cuticle metabolism. From a total of 757 such genes, 43% (326) were present in all tissues, whereas 8% (57) were tissue specific. Of these 57 genes, most (42) were outer epidermis specific (see Supplemental Figure 5 online). Of particular note were 22 genes that were common to both outer and inner epidermal tissues only, most of which were annotated as functionally related with cuticle metabolism (see Supplemental Data Set 4 online).

Almost half of the cuticle-related unigenes were included in the predicted clusters I.B.2.b (129) or II.B (245) where inner and outer epidermal predominant genes, respectively, are grouped (Figure 6). Of the five families of genes that have been proposed to be related with cuticle metabolism, lipid transfer proteins are particularly abundant in the outer epidermis (cluster II.B), together with a strong representation of flavonoid biosynthetic genes in both outer and inner epidermis. These, together with the plant GDSL family and cytochrome P450 and ABC transporter genes, account for almost 80% of the cuticle-related genes in cluster II. B and 75% of those in cluster I.B.2.b.

Identification of a Cuticle Lining the Inner Epidermis of the Pericarp

The expression of so many cuticle metabolism–related genes in both epidermal cell layers suggested that, like the better characterized outer epidermis, the inner epidermis has considerable lipid biosynthetic activity and potentially a cuticular or suberized layer. The presence of a cuticle-like material associated with the inner surface of the tomato pericarp was suggested more than 60 years ago (Kraus, 1949), but since then its existence has been supported only by indirect evidence. Notably, the expression of *Cer6*, a wax biosynthetic gene, was reported in the inner epidermis (Mintz-Oron et al., 2008), and Almeida and Huber (2001) noted the presence of what appeared to be a cuticle-like surface covering the tomato fruit endocarp (sensu stricto, inner epidermis) internal surface following scanning electron microscopy.
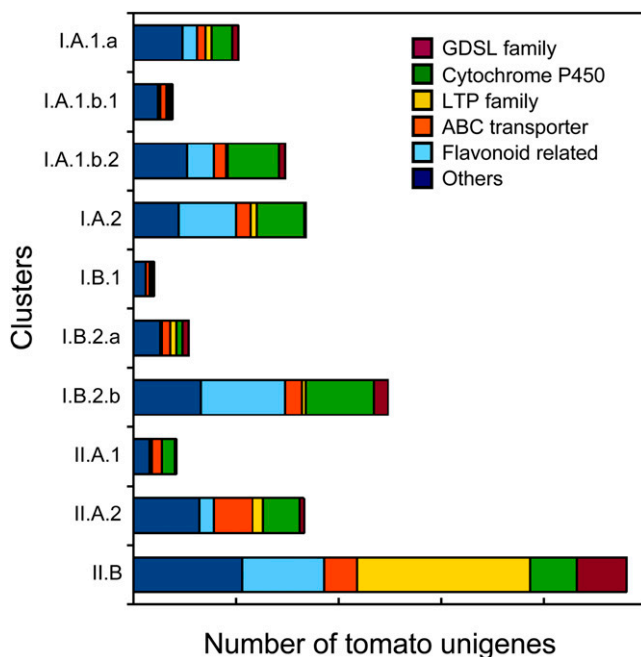

Figure 6. Cluster Distribution of Unigenes Associated with Cuticle Biosynthesis and Structure.

Distribution of unigenes annotated as having a function related to plant cuticles among the predicted hierarchical clusters shown in Figure 3.

We used cryosections of tomato pericarp and a lipid-specific dye to confirm the presence of a lipidic structure associated with the inner epidermis of the pericarp. As a control, Oil Red O was used to stain the outer epidermal cuticle of 10-DPA fruit (cv Ailsa Craig), which appeared as a characteristic continuous bright-red structure, $\sim$0.6 μm thick, covering the outer periclinal cell wall (Figure 7A). A similar structure was observed covering the surface of the inner epidermis facing the locular cavity, with an average thickness of $\sim$0.4 μm (Figure 7B). We also observed similar cuticle-like lipid membranes covering both the outer (Figure 7C) and inner (Figure 7D) epidermal layers of 10-DPA fruit from another tomato cultivar, M82. During M82 fruit development, the outer cuticle increased substantially in thickness and at the mature green (MG) stage extended between the anticlinal walls of the outer epidermal cells, sometimes as far as several underlying cell layers (Figure 7E), as has been reported for M82 fruit (Buda et al., 2009). By contrast, the inner epidermal lipidic membrane of MG fruit showed no change in thickness compared with 10-DPA fruits and did not extend between the anticlinal cell walls.

The permeability and integrity of the inner epidermal lipidic membrane was tested with a dye penetration test, whereby the locule of a bisected fruit (see Supplemental Figure 6A online) was filled with a solution of Toluidine Blue O (see Supplemental Figure 6B online) and then washed with water (see Supplemental Figure 6C online). The dye stains cell walls if there are stomata, pores, or other apertures (see Supplemental Figure 6D online) but does not penetrate hydrophobic membranes, such as the cuticle. The test was applied to M82 fruit at three ripening stages: 10 DPA, MG, and red ripe (RR). This cultivar was selected as the seeds and associated gelatinous membranes are generally not in contact with the inner epidermal surface, which can result in cellular material adhering and consequent positive Toluidine Blue O staining. The inner surface of the pericarp of 10-DPA fruits was impermeable to the dye solution, and no staining was observed (Figures 7G and 7H). By contrast, while no large-scale staining was obtained with MG (Figure 7I) and RR (see Supplemental Figure 6E online) fruits, close inspection revealed small points of staining (Figures 7J and 7K for MG and RR, respectively). These stained regions did not follow any appreciable pattern or appear to be concentrated in any particular region of the inner epidermal surface.

Biochemical and Biomechanical Characterization of the Inner Epidermal Cuticle

We next isolated samples of the inner epidermal layer from three developmental stages of fruit for biochemical and structural analyses. A large number of fruits was required ($\sim$2500, 200, and 250 fruits for 10 DPA, MG, and RR stages, respectively), and the cultivar M82 was used because of the low abundance and fragility of the inner epidermal membrane of Ailsa Craig fruits. This provided sufficient quantities for analysis of monomer composition by gas chromatography–mass spectrometry and polymer molecular structure determination by NMR and Fourier transform infrared spectroscopy (FTIR), allowing comparison with the corresponding characteristics of the outer epidermal cuticle.
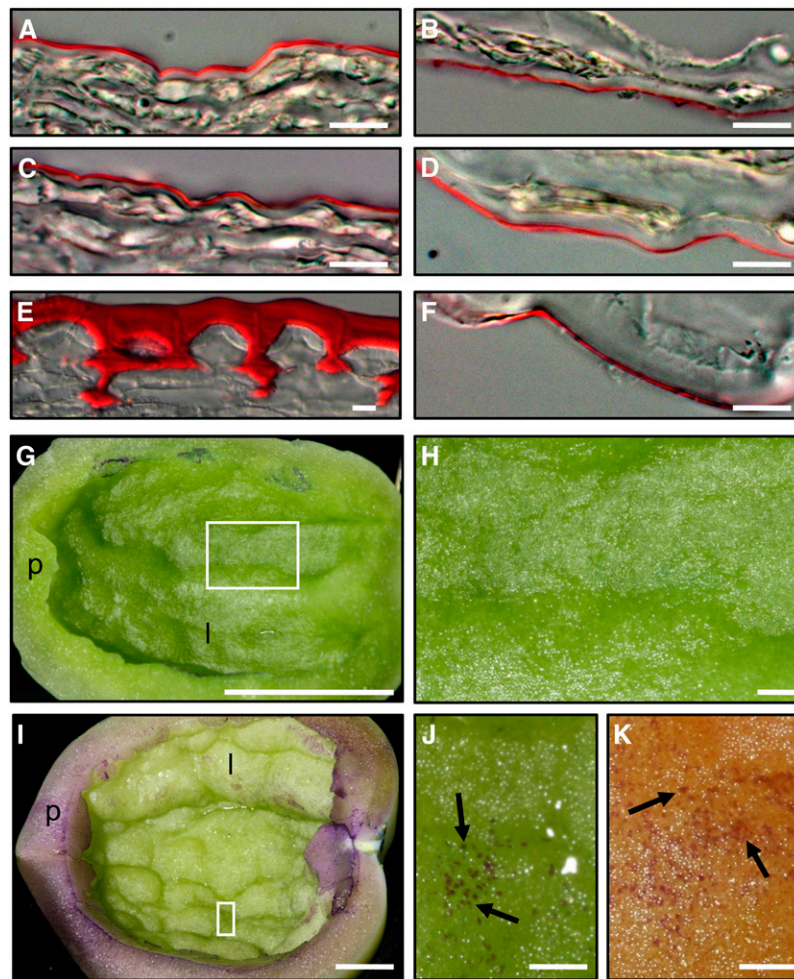
Figure 7. Anatomy and Integrity of the Inner Epidermal Cuticle.

(A), **(C)**, and **(E)** Outer epidermis of the tomato fruit pericarp, showing the cuticle stained with Oil Red O. Fruit from cv Ailsa Craig 10 DPA **(A)** or cv M82 at 10 DPA **(C)** and MG stage **(E)**. Bars = 50 μm in **(A)** and **(C)** and 100 μm in **(E)**.

(B), **(D)**, and **(F)** Inner epidermis of the tomato fruit pericarp, showing the cuticle stained with Oil Red O. Fruit from cv Ailsa Craig at 10 DPA **(B)** or cv M82 at 10 DPA **(D)** and MG stage **(F)**. Bars = 50 μm.

(G) to **(K)** Inner surface of the 10-DPA M82 fruit pericarp following Toluidine Blue dye staining. Bisected fruit showing the pericarp (p) and interior of the locular cavity (l) is shown in **(G)**. The boxed area is shown at greater magnification in **(H)**. Bisected M82 MG fruit **(I)** fruit showing the pericarp (p) and interior of the locular cavity (l). The boxed area is shown at greater magnification in **(J)**. Some of the points of dye penetration are shown (arrows) for both at MG **(J)** and RR **(K)** stage M82 fruits. Bars = 10 mm **in (G)** and **(I)** and 1 mm in **(H)**, **(J)**, and **(K)**.

We applied dewaxing and depolymerization treatments to the inner epidermal lipidic membrane and analyzed the resulting soluble breakdown products by gas chromatography. Two predominant peaks were identified based on their retention behavior and mass spectra (see Supplemental Figure 7A online). The major peak was a derivative of 16-hydroxypalmitic acid, and the second peak was a derivative of 10,16-dihydroxypalmitic acid, both of which are characteristic tomato fruit cutin monomers (Kosma et al., 2010). The same analysis was performed with the outer epidermal cuticle (see Supplemental Figure 7B online), and in this latter case, the 10,16-dihydroxypalmitic acid peak dominated, so the ratio between the two main monomeric constituents is inverted compared with the inner epidermal lipidic

membrane. These findings indicate that the inner membrane is cutin rich and thus structurally similar to the outer cuticle but has a distinctive chemical composition.

The differences in the predominant cutin monomer composition between the inner and the outer cuticles correlated with analysis of the major absorption bands observed by FTIR (see Supplemental Figure 7C online), which again correspond to diagnostic cutin functional groups. Specifically, the inner cuticle showed a lower ratio of bands at 1734 to 2926 cm^{-1} (or 2855 cm^{-1}), which can be assigned to ν (C=O) stretching vibrations of ester groups and ν (CH) stretching vibrations of (CH$_2$)$_n$ groups within fatty acid monomers of the cutin polymer, respectively, and both of which are signatures of ester groups. Another major

difference for the inner cuticles was the reduced intensity of bands at 1061 and 1035 cm^{-1}, which correspond to ν (C-O) alcohol group stretching vibrations, consistent with a lower proportion of midchain hydroxyl groups in the cutin monomer population.

Solid-state NMR analyses revealed further significant structural differences between the outer and inner dewaxed intact cuticles of 10-DPA fruits. Cross-polarization and magic angle spinning solid-state ^{13}C-NMR spectra of the inner and outer dewaxed cuticles confirmed the presence of the expected cuticular functional groups, including long-chain aliphatics (40 to 20 ppm), oxygenated aliphatics (50 to 0 ppm), aromatics and multiply bonded groups (110 to 65 ppm), and carboxyl groups (180 to 170 ppm) (see Supplemental Figure 7D online). The superior spectral resolution of the outer epidermis samples may be attributed to a greater degree of packing order and/or magnetically distinct carbons within the structural building blocks. High-fidelity direct polarization and magic angle spinning (DPMAS) ^{13}C-NMR spectra (Figure 8) indicated the relative proportions of these moieties, including notably diminished intensities of carboxyls and oxygenated aliphatics (CH_2O and CHO) compared with the corresponding waxy cuticles (data not shown). This was an expected result given the presence of long-chain aliphatic acids in the wax component (Isaacson et al., 2009) as well as the artifactual sorption of these intracellular lipids during enzymatic cuticle isolation (Schönherr and Riederer, 1986). The ratio of carboxyls to long-chain aliphatic moieties was comparable to, and slightly greater for, inner versus outer dewaxed cuticles. A similar trend was found for the ratio of total oxygenated aliphatic carbons (CHO and CH_2O) to long-chain aliphatic groups. This finding further emphasizes the cutin-like compositional similarity of the inner and outer membranes. However, the (CHO/CH_2O) ratio was twofold lower for the inner cuticle at the 10-DPA stage, which is in accordance with the gas chromatography–mass spectrometry and FTIR measurements and consistent with a diminished proportion of cross-linkable structural elements in the inner cuticle and the predominance of the 16-hydroxypalmitic acid monomeric constituent.

Differential Expression of Cytochrome P450 Genes in Association with Outer and Inner Epidermal Tissues

The differences observed in cutin monomer composition, with a predominant monohydroxyacid in the inner cuticle, together with the FTIR and NMR data, suggest that the cutin polymers of the inner epidermal cuticle are less cross-linked than those of the outer cuticle. This in turn suggests the involvement of different members of the cytochrome P450 family in the two tissues, as these enzymes have been shown to catalyze the hydroxylation of the cutin monomers. Using the well-defined cutin monomer biosynthetic pathway of Arabidopsis thaliana as a model (Li-Beisson et al., 2009), a cytochrome P450 from the CYP86A subfamily would perform a primary hydroxylation of the omega carbon of the cutin monomer, resulting in the formation of 16-hydroxypalmitic acid. A member of the CYP77A subfamily would then catalyze the secondary hydroxylation at the midchain position, generating 10,16-dihydroxypalmitic acid. Upon search-

ing the outer and inner epidermis unigene expression data sets, we identified several predicted cytochrome P450s, including a CYP86A (TU043403) and two CYP77A genes (TU057365 and TU058169), with spatial expression patterns that matched the differences in monomer composition between the outer and inner epidermal cuticles. While there was no significant difference in the level of expression of the CYP86A putative terminal hydroxylase between the two epidermal layers, transcript abundance of the CYP77A putative midchain hydroxylase was >40 times greater in the outer than inner epidermis (see Supplemental Data Set 1 online).

DISCUSSION

Although high-throughput transcriptome profiling is a common strategy to study complex biological processes, both accuracy and sensitivity are diminished by the fact that RNA samples are typically extracted from homogenized organs, resulting in the mixing of many tissue and cell types. Following protocol optimization, we found that it was possible to use gentle fixation and cryosectioning to preserve fruit pericarp anatomy and obtain tissue type–specific samples via LCM that yielded sufficient levels of RNA for downstream analysis. Two rounds of RNA amplification were necessary for 454 library preparation, but it has been shown previously that this procedure results in no significant relative distortion of the transcript population (Puskás et al., 2002; Nakazono et al., 2003). Coupling LCM with RNA-Seq analysis of multiple adjacent tissues from the same plant organ provided a valuable opportunity to assess the relationship between tissue specialization and the transcriptome landscape across multiple tissues. Moreover, in addition to uncovering spatial patterns of transcript expression, another question was whether LCM together with RNA-Seq can provide a valuable platform for gene discovery, as proved to be the case. Using the samples of microdissected tissues, we obtained a greater than twofold increase in the number of unigenes detected when compared with a similar transcriptome analysis using the whole pericarp of equivalent fruits (J.J. Giovannoni, unpublished data). Interestingly, this proportional increase was much greater for tissue-specific genes, with only four of 217 outer epidermis-specific genes detected in the whole pericarp study. This result supports the idea that dilution of transcripts that are generally low abundance or expressed in tissues or cells that represent small portions of the homogenized tissues are readily overlooked, underscoring the value of tissue and cell specific analyses.

Models of Ubiquitous versus Tissue-Specific Gene Expression

One of the most remarkable observations was the relatively low number of genes (~3%) that were expressed only in a single tissue. An obvious question is whether this reflects substantial contamination among adjacent cell types during the LCM operation. However, several lines of evidence suggest that this is unlikely and that there was a low degree of contamination. First, a similar percentage of ubiquitously expressed transcripts was reported by Birnbaum et al. (2003), who used cell sorting rather than LCM to isolate specific cell types, together with green
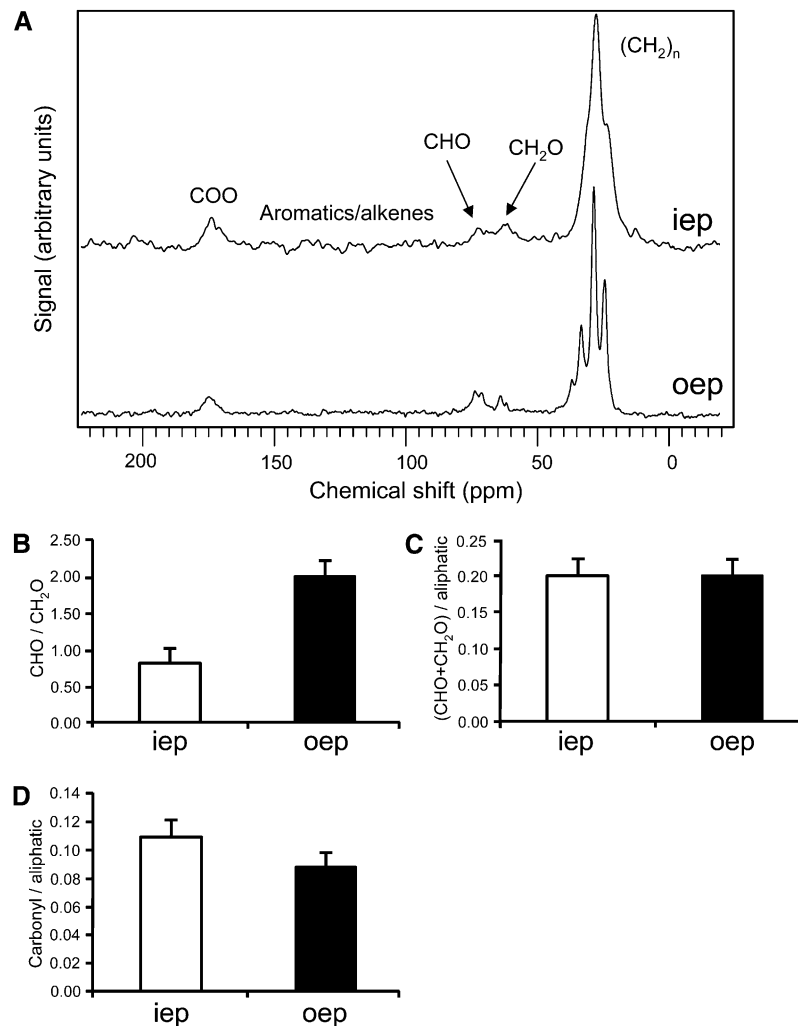
Figure 8. Solid-State NMR Analysis of Isolated Dewaxed Cuticles from 10-DPA Tomato Fruits (cv M82).

(A) The 150-MHz DPMAS ^{13}C-NMR spectra and peak assignments for 10-DPA inner epidermal (iep) and outer epidermal (oep) dewaxed fruit cuticles.
(B) ^{13}C-NMR peak ratios between different oxygenated aliphatic carbon moieties (CHO/CH$_2$O).
(C) ^{13}C-NMR peak ratios of oxygenated aliphatic carbons (CHO+CH$_2$O) to long-chain aliphatics [(CH$_2$)$_n$].
(D) ^{13}C-NMR peak ratios of carbonyl groups (C=O) to long-chain aliphatics [(CH$_2$)$_n$].

fluorescent protein validation of expression patterns. Second, some genes showed extremely large differences in the abundance of specific transcripts in adjacent tissues, while others showed similar relative expression levels. Third, substantial numbers of genes showed expression in two tissues that were not adjacent. The fact that a wide range of expression patterns in different combinations of tissues was seen, with little bias toward overlap in adjacent tissues, further suggests that extensive contamination did not occur and highlights the selectivity of the technique. Conversely, more than half of the detected unigenes were expressed in all tissue types, which again would not be expected as a result of simple contamination of two adjacent tissues.

Taken together, these data suggest that functional specialization of the fruit pericarp tissues is not associated with large populations of genes that show exclusive expression in single tissues. Rather, while subsets of genes are certainly expressed specifically in each tissue examined here, metabolic and regulatory specialization likely results from more subtle and complex control mechanisms. A high proportion of ubiquitously expressed transcripts has been reported in the RNA-Seq profiling of various mammalian tissues (Ramsköld et al., 2009), suggesting that this may be a common feature of eukaryotes, and other studies have indicated that the numbers of transcripts and proteins that are universally expressed are underestimated (Emig and Albrecht, 2011). One recent report suggested that gene expression in metazoans can be divided into two classes: nonfunctional transcripts that are universally expressed at low levels, possibly due to stochastic leaky expression, and those that are expressed at higher levels, estimated at more than one transcript per cell, with a greater functionality (Hebenstreit et al., 2011).

Our data are congruent with this newly emerging view, which has in large part resulted from the remarkable sensitivity provided by new sequencing technologies.

Tissue-Associated Transcriptome Profiling Reveals Diverse Patterns of Functional Specialization

Analysis of the broad patterns of transcript expression data, as well as targeting of specific molecular pathways, revealed underlying trends in terms of the degree of functional specialization and also highlighted specific processes that are unique or common to the various pericarp tissues. Conclusions were drawn from both qualitative and quantitative clustering analyses of individual transcripts across all five tissues, from examining pairwise combinations of tissues, and by assessing both individual transcript annotations and the GO categorizations.

We evaluated the expression of suites of both regulatory and structural genes, focusing particularly on those with a known connection to processes that are prominent during fruit expansion. For example, analysis of the families of GT and GH genes that contribute to polysaccharide synthesis and disassembly, respectively, showed that most genes show a ubiquitous spatial expression, which is contrary to the commonly proposed explanation for the detection of multiple members of the same family in homogenized tissue. Instead, our data support a model where different isozymes from a particular GT or GH family have functional differences (such as substrate specificity), enzymatic properties, or unique modes of regulation. However, we note that the GT and GH profiles of the outer epidermis and vascular tissues show the greatest differences, suggesting distinct wall compositions or structures. This is certainly the case for xylem cells of the vascular bundle, which have elaborated and thickened secondary walls.

Another major target of interest in this study was patterns of genes associated with energy metabolism in the expanding fruit. The collenchyma and parenchyma constitute the main metabolic factories in the fruit pericarp, even at this early developmental stage, and the spatial patterns of transcript expression largely mirror what would be anticipated from many previous biological and/or physiological studies. For example, there are generally reciprocal changes in the expression of genes associated with photosynthesis and photorespiration versus those encoding enzymes of the TCA cycle and elements of alternative respiration. This trend is apparent at the pathway level, but some important points should be noted. First, these changes are largely quantitative, with the major pathways of energy metabolism being present in all tissue types. This observation is consistent with a previous microarray study (Lemaire-Chamley et al., 2005) of early tomato fruit development that detected a surprisingly large number of photosynthetic genes in tissues where expression was unanticipated, based on morphological and physiological studies. However, given the broader coverage and greater sensitivity of the approach taken here, we were able to perform a far more comprehensive survey.

The data presented here also support the previous observation that collenchyma tissues can function as a site of starch synthesis. However, it is interesting to note that only the inner epidermis shows significantly lower expression of starch synthesis–related transcripts than the collenchyma, suggesting that the other tissues maintain some capacity to synthesize starch as an energy reserve. This is certainly true for the parenchyma (Beckles et al., 2001; Centeno et al., 2011) but has yet to be demonstrated in the other pericarp tissues. With regard to photosynthesis, it is important to note that the presence of transcripts corresponding to most of the photosynthesis-associated pathways in all tissues studied does not imply that their functions are identical in all tissue types. Indeed, the lower expression levels of genes associated with photosynthesis and photorespiration in the parenchyma, as well as genes related to photosystems, suggests that it is highly unlikely that photosynthesis occurs in this tissue. Consistent with this observation, a large number of assimilate transporters are expressed at relatively high levels in the vascular tissues, as are the pathways of Suc degradation and the TCA cycle; all of these features are suggestive of a heterotrophic sink (Weigelt et al., 2008). Both inner and outer epidermal tissues also displayed elevated levels of assimilate transporters. Taken together, these data strongly suggest source sink gradients between several of the tissue types under study. While these data are entirely supported by current knowledge of tissue function, it will be important to test these findings once sufficiently sensitive methods have been developed to allow comprehensive and accurate metabolic flux profiling.

In addition to primary metabolism, we also targeted pathways associated with secondary metabolites that are known to be important in fruit biology. Flavonoids, such as flavonol and naringin glycosides, accumulate to high levels in the outer epidermis of tomato fruit (Moco et al., 2007; Iijima et al., 2008; Mintz-Oron et al., 2008; Adato et al., 2009), and some of the associated genes have also been reported to show outer epidermis predominant expression (Mintz-Oron et al., 2008). Since transcript levels of flavonoid related genes, such as the transcription factor *MYB12* (Adato et al., 2009; Ballester et al., 2010), were highly expressed in the outer epidermis (see Supplemental Figure 3 online), tissue specificities for production and accumulation were well correlated in the case of flavonoids in tomato fruits.

Identification and Analysis of an Internal Fruit Cuticle

While the collenchyma and parenchyma show the greatest proportion of commonly expressed genes and the smallest of tissue-specific genes, the vascular tissues and outer epidermal tissues showed evidence of the greatest functional specialization. This is reflected morphologically, with the thickened cell walls of many vascular cells, and by the deposition of a thick cuticle by the outer epidermal layer. Accordingly, a major feature of the transcript profiles of the outer epidermal cells was a large number of genes associated with cuticle formation, which represents a major biosynthetic process at this fruit developmental stage. However, a striking and unanticipated result was the expression of large numbers of cuticle-associated genes in the inner epidermis, or in both epidermal

cell layers, together with many genes that are described as "predicted" or "unknown." We interpreted this to suggest that the inner epidermis might synthesize an inner cuticle that has some structural and compositional features in common with the outer epidermal cuticle.

The tomato fruit pericarp develops from the carpels of the flower, organs that are believed to be modified leaves in terms of their ontogeny (Esau, 1965). In the fruit pericarp, the leaves have two surfaces, with the inner and outer epidermis corresponding to the adaxial and abaxial leaf surfaces, respectively. Distinct differences in the adaxial and abaxial cuticle composition of leaves have previously been noted (Holloway, 1973; Ringelmann et al., 2009), and in this study, we confirmed that the inner epidermal cells form a thin cuticle with a cutin composition that differs from that of the far thicker outer epidermal cuticle. In this regard, the ontogeny of the fruit pericarp as a modified leaf is revealed. The inner epidermis cutin, shown by FTIR spectroscopy to exhibit a typical polyester structure, is primarily composed of 16-hydroxypalmitic acid, and the outer epidermis is rich in 10,16-dihydroxypalmitic acid. This difference is likely attributed to the relative expression of a midchain hydroxylase of the CYP77A subfamily, the transcript levels of which are 40 times greater in the outer than inner epidermis. Without a secondary hydroxyl, the inner epidermis cutin matrix is likely more linear and more extensible.

Whether the inner epidermis has a physiological function or is merely vestigial in nature is currently under investigation. Although it is likely not important as a transpiration or pathogen barrier in intact fruit, this inner membrane could influence water movement in the pericarp and, consequently, turgor pressure and fruit tissue biomechanical properties (Saladié et al., 2007). Almeida and Huber (2001) reported that the inner epidermal cell layer (referred to in their study as the endocarp) of MG tomato fruit (cv Sun Coast) had apertures that became occluded during fruit ripening. They further suggested that this process might affect movement of gases or fluids between the locular cavity and the pericarp. We saw the opposite pattern in M82 and Ailsa Craig tomato fruits, in that the cuticles of expanding fruits were impermeable to aqueous liquids, but apertures were present in MG and ripening fruits. Whether this reflects a difference in cultivar or environmental conditions remains to be determined. Another function of the inner cuticle might be to establish a structural boundary between the pericarp and the locule during early fruit development and prevent tissue fusion, as is the case for the cuticle of other organs (Javelle et al., 2011). This work establishes that there are both common and specialized suites of genes that are associated with the biosynthesis of the inner and outer epidermal cuticles, and targeted disruption and ectopic expression of genes from both classes should reveal the significance of this specialization.

To conclude, this study provides insights into global transcriptome patterns in a complex plant organ and demonstrates the great value of tissue-specific gene expression profiling as a means to resolve spatial variation in tissue and organ developmental regulation and metabolic specialization. In addition, we illustrate the utility of such an approach as a mechanism for gene discovery and as a platform for research into fundamental aspects of plant development and biology.

METHODS

Fruit Pericarp Tissue Preparation for LCM Harvest

Tomato (*Solanum lycopersicum* cv Ailsa Craig) plants were grown in a greenhouse in Ithaca, NY, under 16 h of light and 8 h of dark, using standard practices. Fruits were harvested at 10 DPA, and a ring of pericarp (Figure 1), ~3 mm wide, was separated from the equatorial region of each tomato fruit and divided into 3×3-mm cubes. Three fruit were harvested, one from each of three different plants, and the cubed material was mixed before being prepared for sectioning. This was repeated three times, providing material from nine different fruits divided among three independent biological pools. The cubed pericarp material was immediately transferred to 75% (v/v) ethanol and 25% (v/v) acetic acid, at a 1:10 volume ratio of tissue to fixative, on ice following Nakazono et al. (2003), with some modifications. The fixative was infiltrated into the tissue cubes under vacuum for 15 min on ice and then replaced with fresh solution, before leaving on a rotator at 4°C overnight. Tissue cubes were transferred to 10% (w/v) Suc and prepared with diethyl pyrocarbonate–treated PBS buffer (137 mM NaCl, 8 mM Na_2HPO_4, 2.7 mM KCl, and 1.5 mM KH_2PO_4, pH 7.3) to reduce ice crystal formation. The tissue cubes were then infiltrated with Suc solution under vacuum on ice for 15 min and the vials rotated at 4°C until the cubes were fully submerged. The Suc solution was then exchanged for 20% (w/v) Suc, prepared as described above, and the infiltration/rotating steps repeated as before. The tissue cubes were washed in OCT medium (Sakura) and transferred to cryomolds filled with OCT medium, frozen in a glass beaker chilled over liquid nitrogen, and stored at −80°C.

Laser Microdissection, RNA Amplification, and cDNA Synthesis

Pericarp tissue cubes were sectioned in a cryostat (Microm HM550; ThermoFisher Scientific) and mounted on an adhesive-coated slide using the CryoJane transfer system (Instrumedics) at −26°C, as described by Nakazono et al. (2003). The frozen slides were immediately incubated in 70% (v/v) ethanol at −20°C for 1 min, followed by dehydration steps of 0.5 to 1 min each in 95% (v/v) ethanol and 100% (v/v) ethanol, and twice in xylene (2 min each). Sections were air dried and used intermediately for LCM.

Laser microdissection was performed using a P.A.L.M. Laser Microbeam (P.A.L.M. Microlaser Technologies). Pericarp tissues were captured from 5 to 10 sections per sample and comprised 2 to 16 mm^2 of tissue with a section thickness of 10 μm for the inner and outer epidermis and 16 μm for the other tissues. Three biological replicates were obtained for each tissue. Total RNA was isolated using an RNeasy Micro Kit (Qiagen), and mRNA was amplified as described by Matas et al. (2010) in a two-round amplification with the TargetAmp system (Epicenter Biotechnologies), following the manufacturer's instructions. cDNA libraries were prepared for each tissue from the amplified RNA using the SuperScript Choice system (Invitrogen), and the double-strand cDNA was purified with a PureLink PCR purification kit (Invitrogen).

454 Sequencing and Sequence Assembly

Approximately 5 μg of cDNA (a pool of the three biological replicates) of each of the pericarp tissue samples was used for sequencing on a GS-FLX platform (Roche Diagnostics). A half-plate sequencing run was performed for each sample following the manufacturer's protocols. The raw 454 sequence files in SFF format were base called using the Pyrobayes base caller (Quinlan et al., 2008). The sequences were then processed to remove low-quality regions and adaptor sequences using LUCY (Chou and Holmes, 2001) and SeqClean (http://compbio.dfci. harvard.edu/tgi/software). The resulting high-quality sequences were

then screened against the NCBI UniVec database, *Escherichia coli* genome sequences and tomato rRNA, to remove possible contaminating sequences. Sequences shorter than 30 bp were discarded. Tomato cDNA sequences were assembled into unigenes using the iAssembler program (http://bioinfo.bti.cornell.edu/tool/iAssembler) as described by Guo et al. (2010) and combined with similar EST libraries derived from various tomato organs and tissues, as listed at http://ted.bti.cornell.edu/cgi-bin/TFGD/digital/sample.cgi?ID=D002.

Unigene Annotation and Pathway Prediction

Tomato unigenes were searched using BLAST against GenBank nonredundant protein (nr) and UniProt databases with a cutoff e value of $1 e^{-5}$. The unigene sequences were also translated into proteins using ESTScan (Iseli et al., 1999), and the translated protein sequences were then compared with InterPro (http://www.ebi.ac.uk/interpro) and Pfam (http://pfam.sanger.ac.uk) domain databases. The GO terms were assigned to each unigene based on the GO terms annotated to its corresponding homologs in the UniProt database (Camon et al., 2004), as well as those to InterPro and Pfam domains using interpro2go and pfam2go mapping files provided by the GO website (http://www.geneontology.org), respectively. The GO annotations of tomato unigenes were mapped to the plant-specific GO slim ontology using the map2slim script (http://www.geneontology.org/GO.slims.shtml), and the unigenes were classified into different functional groups based on these GO slims. The annotations of tomato unigenes were then formatted into the PathoLogic format and used to predict biochemical pathways using the Pathway Tools (Karp et al., 2002).

Identification of Differentially Expressed Genes

Following cDNA sequence assembly, digital expression information for each unigene was derived following normalization to the total number of sequenced transcripts per sample. Significance of differential gene expression was determined using R following the method described by Stekel et al. (2000), and the resulting raw P values were adjusted for multiple testing using the false discovery rate (FDR; Benjamini and Hochberg, 1995). Genes with fold change > 2 and FDR < 0.05 were designated as differentially expressed genes. GO terms enriched in the set of differentially expressed genes were identified using GO::Term-Finder (Boyle et al., 2004), requiring P values adjusted for multiple testing (FDR; Benjamini and Hochberg, 1995) to be < 0. Changed biochemical pathways were identified using the Plant MetGenMAP system (Joung et al., 2009). To identify groups of genes that have similar expression patterns, we performed hierarchical clustering using the expression values from each tomato tissue/cell type. The analysis was conducted using software routines from MATLAB (version 7.8, R2009a) with Pearson correlation as the distance measure. The cluster tree was then divided into distinct clusters, each of which contained genes with a unique expression profile by visual inspection.

Pericarp Anatomy, Histology, and Cuticle Analysis

Tomato (cv Ailsa Craig and cv M82) plants were grown in an open field during a summer season in Freeville, NY, using standard practices and their fruits used for microscopy studies and cuticle isolation. Fruits of both cultivars were harvested at the 10-DPA stage, at the MG stage when fruits reached full size but were still green, and at the RR stage, which was 4 to 5 d after the color break. Tissue was harvested, fixed, cryoprotected, and embedded as outlined by Buda et al. (2009). Cryosections (4-μm thick) of each tomato sample were cut and melted at room temperature onto VistaVision HistoBond slides (VWR). Each slide was dried at room temperature overnight and then heated at 200°C on a hot plate for ~1 min prior to staining.

Oil Red O Staining and Microscopy

Oil Red O (Alfa Aesar) stock solution (saturated in isopropyl alcohol) was diluted 3:2 with distilled water and filtered through a 0.45-μm pore diameter syringe filter. The stain was added to the slides for 30 min. The slides were taken sequentially through an alcohol series of 50, 30, 22, 15, and 8% isopropyl alcohol and mounted in 8% isopropyl alcohol with a cover slip, sealed with hot LPV (1:1:1 mixture of lanolin to paraffin to Vaseline), and viewed immediately. Tissue sections were imaged with a Zeiss AxioImager A1 microscope (Zeiss) equipped with a Zeiss EC-Plan NeoFluar ×100/1.3 oil immersion objective, a Zeiss AxioCam MRc color video camera, and Zeiss AXIOVs40 4.6.3.0 software. Images were taken using Nomarski optics (differential interference contrast) with the polarizer and analyzer set to extinction.

Toluidine Blue Dye Penetration Test

The method for examination of cuticular integrity was adapted from Tanaka et al. (2004). An aqueous solution of 0.01% (w/v) Toluidine Blue O (Sigma-Aldrich), previously filtered through a PTFE membrane filter (0.45-μm pore diameter; Whatman), was poured into the fruit inner locular cavity, after the seeds were removed, until completely filled. In fruit with two or more locules, one of the locules was used for the test and the other one was filled with water as the negative control. After 2 min, the Toluidine Blue O solution was removed and the inner surface of the locule was rinsed with water to remove excess Toluidine Blue O solution. Small holes in the surface were produced with a pin to allow penetration of the dye in discrete areas as the positive control.

Enzymatic Cuticle Isolation

Cuticle isolation followed the method described by Isaacson et al. (2009) except that the period of incubation in enzymatic isolation buffer was up to 4 months, and shaking of the container was avoided to prevent sample fragmentation. To avoid mixing of outer and inner cuticles, in 10-DPA fruits the outer cuticle was removed manually using a sharp razor before sectioning the pericarp. For MG and RR fruits, the pericarp was divided in two pieces longitudinally and incubated separately. Approximately 2500 10-DPA fruits and 200 fruits each for MG and RR of the M82 cultivar were needed to obtain enough isolated inner cuticle for the analysis. Isolated membranes were removed manually from the isolation buffer and dried at room temperature.

Solid-State NMR Spectroscopy

Compositional analyses of dewaxed 10-DPA M82 tomato cuticles were performed using solid-state NMR spectroscopy. The dewaxed cuticle samples were obtained by removing the waxes and other soluble materials from the intact cuticles with a Soxhlet extraction using three successive solvents of varying polarity: methanol, chloroform, and hexane. A standard Soxhlet apparatus with a glass extraction thimble (Synthware) was used to achieve exhaustive extraction without significant sample losses. ^{13}C magic angle spinning NMR measurements were performed at a typical spinning speed of 10 kHz ($\pm$20 Hz), including cross-polarization and magic angle spinning experiments with a spin-lock time of 1 to 1.5 ms and a 3-s recycle delay between successive acquisitions to identify molecular groups and direct polarization (DPMAS) experiments with a recycle delay of 100 s to make quantitative assessments of the various carbon moieties. High-power heteronuclear proton decoupling was achieved using the SPINAL method (Fung et al., 2000) with ^{1}H field strengths corresponding to 57 and 185 kHz in separate experiments. A Varian VNMRS NMR spectrometer operating at a ^{1}H frequency of 600 MHz and equipped with a fastMAS probe was used to

carry out MAS experiments on both intact and dewaxed cuticles (1 to 4 mg of powdered samples). All spectral data were processed with 100 to 200 Hz line broadening and analyzed independently using VNMRJ (version 2.2C; Agilent Technologies) and Spinworks (version 3.1.7; ftp://davinci.chem.umanitoba.ca/pub/marat/SpinWorks/) software. Chemical shifts were referenced externally to the methylene (-CH$_2$-) group of adamantane (Sigma-Aldrich) at 38.48 ppm. The relative proportions of the various functional groups were obtained by comparing integrated regions of the ^{13}C DPMAS spectra. Experimental error limits were evaluated by repeating DPMAS measurements at two different ^{1}H decoupling powers for both inner and outer dewaxed cuticles. In addition, error limits for the compositional analyses were determined from experiments on replicate RR outer dewaxed cuticle samples, as described by Isaacson et al. (2009) for the M82 cultivar.

Gas Chromatography–Mass Spectrometry

Isolated cuticular membranes from the outer or inner epidermis were extracted three times with chloroform and depolymerized with anyhdrous sodium methoxide as described by Bonaventure et al. (2004) with minor modifications: The internal standards were omitted, the methyl esters of the cutin monomers were recovered in diethyl ether, and this extract was dried using dimethoxypropane. After evaporation under nitrogen, the products were trimethylsilyl derivatized by heating to 90°C for 10 min with 10 μL of N,O-bis(trimethylsilyl)-trifluoroacetamide and 10 μL of pyridine. Products were then analyzed using an Agilent 6850 GC equipped with cool-on-column injector, HP-1 column (30 m × 0.32 mm × 0.1-μm film thickness), and flame ionization detector. The identities of major peaks were confirmed by running the same samples using split injection on an Agilent 6890 GC equipped with a Supelco JEOL GCMate mass spectrometer running in electron impact mode.

FTIR Spectroscopy

Infrared spectra were recorded on a Nicolet MAGNA-IR 560 spectrometer with a resolution of 4.0 from 524.6 to 3999.7 cm^{-1} for dry isolated samples of outer and inner dewaxed cuticle. For each sample, 400 interferograms were coadded to generate the FTIR spectrum.

Accession Numbers

Sequence data described in this article can be found in the GenBank Sequence Read Archive data library under accession number SRP004923. The assembled sequences of the unigene and the digital expression values were deposited at the Tomato Functional Genomics Database (http://ted.bti.cornell.edu/cgi-bin/TFGD/digital/home.cgi).

Supplemental Data

The following materials are available in the online version of this article.

Supplemental Figure 1. GO Term Functional Annotation of Tomato Transcripts Showing Pericarp Tissue–Associated Expression.

Supplemental Figure 2. Expression Profiles of Putative Transcription Factors in Tomato Fruit Pericarp Tissues.

Supplemental Figure 3. Relative Expression in Different Pericarp Tissues of Transcripts Associated with Flavonoid Biosynthesis.

Supplemental Figure 4. Expression Profiles of Cell Wall–Associated Genes in Tomato Fruit Pericarp Tissues.

Supplemental Figure 5. Expression Profiles of Cuticle-Associated Genes in Tomato Fruit Pericarp Tissues.

Supplemental Figure 6. Toluidine Blue Dye Penetration Test.

Supplemental Figure 7. Composition and Structural Characterization of Isolated, Dewaxed Inner and Outer Epidermis of the Pericarp Cuticles.

Supplemental Table 1. Number of Sequence Reads with 454 GS-FLX for Each LCM Tomato Pericarp Tissue.

Supplemental Data Set 1. Summary of the Assembled Unigenes.

Supplemental Data Set 2. Number of Upregulated and Downregulated Genes (FDR < 0.05) in Each Predicted Cluster in the Six Pairwise Comparisons.

Supplemental Data Set 3. Summary of the Annotated Transcription Factors.

Supplemental Data Set 4. Transcripts That Were Detected Only in the Outer Epidermis, Inner Epidermis, or Both, Showing Best BLAST Match in Genbank and the Associated e Value Score.

AUTHOR CONTRIBUTIONS

A.J.M. designed and performed research, contributed new analytic/computational tools, analyzed data, and cowrote the article. T.H.Y. and G.J.B. performed research, analyzed data, and cowrote the article. Y.Z., S.C., L.P., A. Adato, and A. Aharoni performed research and analyzed data. R.S., A.R.F., J.J.G., and J.K.C.R. designed research, analyzed data, and cowrote the article. Z.F. designed research, contributed new analytic/computational tools, analyzed data, and cowrote the article.

REFERENCES

Adato, A., et al. (2009). Fruit-surface flavonoid accumulation in tomato is controlled by a SlMYB12-regulated transcriptional network. PLoS Genet. **5:** e1000777.

Agustí, J., Merelo, P., Cercós, M., Tadeo, F.R., and Talón, M. (2009). Comparative transcriptional survey between laser-microdissected cells from laminar abscission zone and petiolar cortical tissue during ethylene-promoted abscission in citrus leaves. BMC Plant Biol. **9:** 127.

Alba, R., et al. (2004). ESTs, cDNA microarrays, and gene expression profiling: tools for dissecting plant physiology and development. Plant J. **39:** 697–714.

Alba, R., Payton, P., Fei, Z.J., McQuinn, R., Debbie, P., Martin, G.B., Tanksley, S.D., and Giovannoni, J.J. (2005). Transcriptome and selected metabolite analyses reveal multiple points of ethylene control during tomato fruit development. Plant Cell **17:** 2954–2965.

Almeida, D.P.F., and Huber, D.J. (2001). Transient increase in locular pressure and occlusion of endocarpic apertures in ripening tomato fruit. J. Plant Physiol. **158:** 199–203.

Ballester, A.-R., et al. (2010). Biochemical and molecular analysis of pink tomatoes: Deregulated expression of the gene encoding transcription factor *SlMYB12* leads to pink tomato fruit color. Plant Physiol. **152:** 71–84.

Bauwe, H., Hagemann, M., and Fernie, A.R. (2010). Photorespiration: Players, partners and origin. Trends Plant Sci. **15:** 330–336.

Beckles, D.M., Smith, A.M., and ap Rees, T. (2001). A cytosolic ADP-glucose pyrophosphorylase is a feature of graminaceous endosperms, but not of other starch-storing organs. Plant Physiol. **125:** 818–827.

Benjamini, Y., and Hochberg, Y. (1995). Controlling the false discovery rate - A practical and powerful approach to multiple testing. J. R. Stat. Soc. Series B Stat. Methodol. **57:** 289–300.

Bino, R.J., Ric de Vos, C.H., Lieberman, M., Hall, R.D., Bovy, A., Jonker, H.H., Tikunov, Y., Lommen, A., Moco, S., and Levin, I. (2005). The light-hyperresponsive *high pigment-2^{dg}* mutation of tomato: Alterations in the fruit metabolome. New Phytol. **166:** 427–438.

Birnbaum, K., Shasha, D.E., Wang, J.Y., Jung, J.W., Lambert, G.M., Galbraith, D.W., and Benfey, P.N. (2003). A gene expression map of the *Arabidopsis* root. Science **302:** 1956–1960.

Bombarely, A., Menda, N., Tecle, I.Y., Buels, R.M., Strickler, S., Fischer-York, T., Pujar, A., Leto, J., Gosselin, J., and Mueller, L.A. (2011). The Sol Genomics Network (solgenomics.net): Growing tomatoes using Perl. Nucleic Acids Res. **39**(Database issue): D1149–D1155.

Bonaventure, G., Beisson, F., Ohlrogge, J., and Pollard, M. (2004). Analysis of the aliphatic monomer composition of polyesters associated with *Arabidopsis* epidermis: Occurrence of octadeca-*cis*-6, *cis*-9-diene-1,18-dioate as the major component. Plant J. **40:** 920–930.

Boyle, E.I., Weng, S.A., Gollub, J., Jin, H., Botstein, D., Cherry, J.M., and Sherlock, G. (2004). GO:TermFinder—Open source software for accessing Gene Ontology information and finding significantly enriched Gene Ontology terms associated with a list of genes. Bioinformatics **20:** 3710–3715.

Brooks III, L., et al. (2009). Microdissection of shoot meristem functional domains. PLoS Genet. **5:** e1000476.

Brummell, D.A. (2006). Cell wall disassembly in ripening fruit. Funct. Plant Biol. **33:** 103–119.

Buda, G.J., Isaacson, T., Matas, A.J., Paolillo, D.J., and Rose, J.K.C. (2009). Three-dimensional imaging of plant cuticle architecture using confocal scanning laser microscopy. Plant J. **60:** 378–385.

Cai, S., and Lashbrook, C.C. (2008). Stamen abscission zone transcriptome profiling reveals new candidates for abscission control: enhanced retention of floral organs in transgenic plants overexpressing Arabidopsis *ZINC FINGER PROTEIN2*. Plant Physiol. **146:** 1305–1321.

Camon, E., Magrane, M., Barrell, D., Lee, V., Dimmer, E., Maslen, J., Binns, D., Harte, N., Lopez, R., and Apweiler, R. (2004). The Gene Ontology Annotation (GOA) Database: Sharing knowledge in Uniprot with Gene Ontology. Nucleic Acids Res. **32**(Database issue): D262–D266.

Carrari, F., Baxter, C., Usadel, B., Urbanczyk-Wochniak, E., Zanor, M.I., Nunes-Nesi, A., Nikiforova, V., Centero, D., Ratzka, A., Pauly, M., Sweetlove, L.J., and Fernie, A.R. (2006). Integrated analysis of metabolite and transcript levels reveals the metabolic shifts that underlie tomato fruit development and highlight regulatory aspects of metabolic network behavior. Plant Physiol. **142:** 1380–1396.

Carrari, F., and Fernie, A.R. (2006). Metabolic regulation underlying tomato fruit development. J. Exp. Bot. **57:** 1883–1897.

Catalá, C., Howe, K.J., Hucko, S., Rose, J.K.C., and Thannhauser, T.W. (2011). Towards characterization of the glycoproteome of tomato (*Solanum lycopersicum*) fruit using Concanavalin A lectin affinity chromatography and LC-MALDI-MS/MS analysis. Proteomics **11:** 1530–1544.

Centeno, D.C., et al. (2011). Malate plays a crucial role in starch metabolism, ripening, and soluble solid content of tomato fruit and affects postharvest softening. Plant Cell **23:** 162–184.

Chou, H.H., and Holmes, M.H. (2001). DNA sequence quality trimming and vector removal. Bioinformatics **17:** 1093–1104.

Emig, D., and Albrecht, M. (2011). Tissue-specific proteins and functional implications. J. Proteome Res. **10:** 1893–1903.

Esau, K. (1965). Plant Anatomy, 2nd ed. (New York: Wiley).

Faurobert, M., Mihr, C., Bertin, N., Pawlowski, T., Negroni, L., Sommerer, N., and Causse, M. (2007). Major proteome variations associated with cherry tomato pericarp development and ripening. Plant Physiol. **143:** 1327–1346.

Fei, Z.J., Joung, J.G., Tang, X.M., Zheng, Y., Huang, M.Y., Lee, J.M., McQuinn, R., Tieman, D.M., Alba, R., Klee, H.J., and Giovannoni, J.J. (2011). Tomato Functional Genomics Database: A comprehensive resource and analysis package for tomato functional genomics. Nucleic Acids Res. **39**(Database issue): D1156–D1163.

Fung, B.M., Khitrin, A.K., and Ermolaev, K. (2000). An improved broadband decoupling sequence for liquid crystals and solids. J. Magn. Reson. **142:** 97–101.

Giovannoni, J.J. (2004). Genetic regulation of fruit development and ripening. Plant Cell **16** (suppl.): S170–S180.

Guo, S.G., Zheng, Y., Joung, J.G., Liu, S.Q., Zhang, Z.H., Crasta, O.R., Sobral, B.W., Xu, Y., Huang, S.W., and Fei, Z.J. (2010). Transcriptome sequencing and comparative analysis of cucumber flowers with different sex types. BMC Genomics **11:** 384.

Gur, A., Semel, Y., Cahaner, A., and Zamit, D. (2004). Real time QTL of complex phenotypes in tomato interspecific introgression lines. Trends Plant Sci. **9:** 107–109.

Hebenstreit, D., Fang, M., Gu, M., Charoensawan, V., van Oudenaarden, A., and Teichmann, S.A. (2011). RNA sequencing reveals two major classes of gene expression levels in metazoan cells. Mol. Syst. Biol. **7:** 497.

Holloway, P.J. (1973). Cutins of *Malus pumila* fruits and leaves. Phytochemistry **12:** 2913–2920.

Howe, E., Holton, K., Nair, S., Schlauch, D., Sinha, R., Quackenbush, J., Ochs, M.F., Casagrande, J.T., and Davuluri, R.V. (2010). MeV: MultiExperiment Viewer. In Biomedical Informatics for Cancer Research. (New York: Springer), pp. 267–277.

Huysamer, M., Greve, L.C., and Labavitch, J.M. (1997). Cell wall metabolism in ripening fruit. 8. Cell wall composition and synthetic capacity of two regions of the outer pericarp of mature green and red ripe cv. Jackpot tomatoes. Physiol. Plant. **101:** 314–322.

Iijima, Y., et al. (2008). Metabolite annotations based on the integration of mass spectral information. Plant J. **54:** 949–962.

Isaacson, T., Kosma, D.K., Matas, A.J., Buda, G.J., He, Y.H., Yu, B.W., Pravitasari, A., Batteas, J.D., Stark, R.E., Jenks, M.A., and Rose, J.K.C. (2009). Cutin deficiency in the tomato fruit cuticle consistently affects resistance to microbial infection and biomechanical properties, but not transpirational water loss. Plant J. **60:** 363–377.

Iseli, C., Jongeneel, C.V., and Bucher, P. (1999). ESTScan: A program for detecting, evaluating, and reconstructing potential coding regions in EST sequences. Proc. Int. Conf. Intell. Syst. Mol. Biol. **1:** 138–148.

Ishizaki, K., Larson, T.R., Schauer, N., Fernie, A.R., Graham, I.A., and Leaver, C.J. (2005). The critical role of *Arabidopsis* electron-transfer flavoprotein:ubiquinone oxidoreductase during dark-induced starvation. Plant Cell **17:** 2587–2600.

Itkin, M., Seybold, H., Breitel, D., Rogachev, I., Meir, S., and Aharoni, A. (2009). TOMATO AGAMOUS-LIKE 1 is a component of the fruit ripening regulatory network. Plant J. **60:** 1081–1095.

Javelle, M., Vernoud, V., Rogowsky, P.M., and Ingram, G.C. (2011). Epidermis: The formation and functions of a fundamental plant tissue. New Phytol. **189:** 17–39.

Jiao, Y.L., et al. (2009). A transcriptome atlas of rice cell types uncovers cellular, functional and developmental hierarchies. Nat. Genet. **41:** 258–263.

Joung, J.G., Corbett, A.M., Fellman, S.M., Tieman, D.M., Klee, H.J., Giovannoni, J.J., and Fei, Z.J. (2009). Plant MetGenMAP: An integrative analysis system for plant systems biology. Plant Physiol. **151:** 1758–1768.

Kahlau, S., and Bock, R. (2008). Plastid transcriptomics and translatomics of tomato fruit development and chloroplast-to-chromoplast differentiation: Chromoplast gene expression largely serves the production of a single protein. Plant Cell **20:** 856–874.

Kanai, S., Ohkura, K., Adu-Gyamfi, J.J., Mohapatra, P.K., Nguyen, N.T., Saneoka, H., and Fujita, K. (2007). Depression of sink activity precedes the inhibition of biomass production in tomato plants subjected to potassium deficiency stress. J. Exp. Bot. **58:** 2917–2928.

Karlova, R., Rosin, F.M., Busscher-Lange, J., Parapunova, V., Do, P.T., Fernie, A.R., Fraser, P.D., Baxter, C., Angenent, G.C., and de Maagd, R.A. (2011). Transcriptome and metabolite profiling show that APETALA2a is a major regulator of tomato fruit ripening. Plant Cell **23:** 923–941.

Karp, P.D., Paley, S., and Romero, P. (2002). The Pathway Tools software. Bioinformatics **18** (suppl. 1): S225–S232.

Klee, H.J. (2010). Improving the flavor of fresh fruits: genomics, biochemistry, and biotechnology. New Phytol. **187:** 44–56.

Kolotilin, I., Koltai, H., Tadmor, Y., Bar-Or, C., Reuveni, M., Meir, A., Nahon, S., Shlomo, H., Chen, L., and Levin, I. (2007). Transcriptional profiling of *high pigment-2^{dg}* tomato mutant links early fruit plastid biogenesis with its overproduction of phytonutrients. Plant Physiol. **145:** 389–401.

Kosma, D.K., Parsons, E.P., Isaacson, T., Lü, S., Rose, J.K.C., and Jenks, M.A. (2010). Fruit cuticle lipid composition during development in tomato ripening mutants. Physiol. Plant. **139:** 107–117.

Kraus, G. (1949). Morphologic-anatomical studies on development-conditioned changes in axis, leaf and ovary in some berry fruits. Oesterr. Bot. Z. **96:** 325–360.

Lemaire-Chamley, M., Petit, J., Garcia, V., Just, D., Baldet, P., Germain, V., Fagard, M., Mouassite, M., Cheniclet, C., and Rothan, C. (2005). Changes in transcriptional profiles are associated with early fruit tissue specialization in tomato. Plant Physiol. **139:** 750–769.

Li-Beisson, Y., Pollard, M., Sauveplane, V., Pinot, F., Ohlrogge, J., and Beisson, F. (2009). Nanoridges that characterize the surface morphology of flowers require the synthesis of cutin polyester. Proc. Natl. Acad. Sci. USA **106:** 22008–22013.

Matas, A.J., Agustí, J., Tadeo, F.R., Talón, M., and Rose, J.K.C. (2010). Tissue-specific transcriptome profiling of the citrus fruit epidermis and subepidermis using laser capture microdissection. J. Exp. Bot. **61:** 3321–3330.

Matas, A.J., Gapper, N.E., Chung, M.-Y., Giovannoni, J.J., and Rose, J.K.C. (2009). Biology and genetic engineering of fruit maturation for enhanced quality and shelf-life. Curr. Opin. Biotechnol. **20:** 197–203.

Maurino, V.G., and Peterhansel, C. (2010). Photorespiration: Current status and approaches for metabolic engineering. Curr. Opin. Plant Biol. **13:** 249–256.

Mintz-Oron, S., Mandel, T., Rogachev, I., Feldberg, L., Lotan, O., Yativ, M., Wang, Z., Jetter, R., Venger, I., Adato, A., and Aharoni, A. (2008). Gene expression and metabolism in tomato fruit surface tissues. Plant Physiol. **147:** 823–851.

Moco, S., Capanoglu, E., Tikunov, Y., Bino, R.J., Boyacioglu, D., Hall, R.D., Vervoort, J., and De Vos, R.C. (2007). Tissue specialization at the metabolite level is perceived during the development of tomato fruit. J. Exp. Bot. **58:** 4131–4146.

Nakazono, M., Qiu, F., Borsuk, L.A., and Schnable, P.S. (2003). Laser-capture microdissection, a tool for the global analysis of gene expression in specific plant cell types: Identification of genes expressed differentially in epidermal cells or vascular tissues of maize. Plant Cell **15:** 583–596.

Nashilevitz, S., et al. (2010). An orange ripening mutant links plastid NAD(P)H dehydrogenase complex activity to central and specialized metabolism during tomato fruit maturation. Plant Cell **22:** 1977–1997.

Nelson, T., Gandotra, N., and Tausta, S.L. (2008). Plant cell types: Reporting and sampling with new technologies. Curr. Opin. Plant Biol. **11:** 567–573.

Osorio, S., Alba, R., Damasceno, C.M.B., Lopez-Casado, G., Lohse, M., Zanor, M.I., Tohge, T., Usadel, B., Rose, J.K.C., Fei, Z., Giovannoni, J.J., and Fernie, A.R. (2011). Systems biology of tomato fruit development: Combined transcript, protein, and metabolite analysis of tomato transcription factor (nor, rin) and ethylene receptor (Nr) mutants reveals novel regulatory interactions. Plant Physiol. **157:** 405–425.

Pan, I.L., McQuinn, R., Giovannoni, J.J., and Irish, V.F. (2010). Functional diversification of AGAMOUS lineage genes in regulating tomato flower and fruit development. J. Exp. Bot. **61:** 1795–1806.

Paran, I., and van der Knaap, E. (2007). Genetic and molecular regulation of fruit and plant domestication traits in tomato and pepper. J. Exp. Bot. **58:** 3841–3852.

Puskás, L.G., Zvara, A., Hackler, L., Jr., and Van Hummelen, P. (2002). RNA amplification results in reproducible microarray data with slight ratio bias. Biotechniques **32:** 1330–1334, 1336, 1338, 1340.

Quinlan, A.R., Stewart, D.A., Strömberg, M.P., and Marth, G.T. (2008). Pyrobayes: An improved base caller for SNP discovery in pyrosequences. Nat. Methods **5:** 179–181.

Ramsköld, D., Wang, E.T., Burge, C.B., and Sandberg, R. (2009). An abundance of ubiquitously expressed genes revealed by tissue transcriptome sequence data. PLoS Comput. Biol. **5:** e1000598.

Ringelmann, A., Riedel, M., Riederer, M., and Hildebrandt, U. (2009). Two sides of a leaf blade: *Blumeria graminis* needs chemical cues in cuticular waxes of *Lolium perenne* for germination and differentiation. Planta **230:** 95–105.

Rose, J.K.C., Catalá, C., Gonzalez-Carranza, Z.H., and Roberts, J. (2003). Plant cell wall disassembly. In The Plant Cell Wall, Annual Plant Reviews Series. J.K.C. Rose, ed (Oxford, UK: Blackwell Publishing), pp. 264–324.

Saladié, M., et al. (2007). A reevaluation of the key factors that influence tomato fruit softening and integrity. Plant Physiol. **144:** 1012–1028.

Schönherr, J., and Riederer, M. (1986). Plant cuticles sorb lipophilic compounds during enzymatic isolation. Plant Cell Environ. **9:** 459–466.

Seymour, G., Poole, M., Manning, K., and King, G.J. (2008). Genetics and epigenetics of fruit development and ripening. Curr. Opin. Plant Biol. **11:** 58–63.

Shahbazi, M., Gilbert, M., Labouré, A.-M., and Kuntz, M. (2007). Dual role of the plastid terminal oxidase in tomato. Plant Physiol. **145:** 691–702.

Steinhauser, M.C., Steinhauser, D., Koehl, K., Carrari, F., Gibon, Y.,

Fernie, A.R., and Stitt, M. (2010). Enzyme activity profiles during fruit development in tomato cultivars and *Solanum pennellii*. Plant Physiol. **153:** 80–98.

Stekel, D.J., Git, Y., and Falciani, F. (2000). The comparison of gene expression from multiple cDNA libraries. Genome Res. **10:** 2055–2061.

Tanaka, T., Tanaka, H., Machida, C., Watanabe, M., and Machida, Y. (2004). A new method for rapid visualization of defects in leaf cuticle reveals five intrinsic patterns of surface defects in *Arabidopsis*. Plant J. **37:** 139–146.

Tanksley, S.D. (2004). The genetic, developmental, and molecular bases of fruit size and shape variation in tomato. Plant Cell **16** (suppl.): S181–S189.

Vega-García, M.O., López-Espinoza, G., Chávez Ontiveros, J., Caro-Corrales, J.J., Delgado Vargas, F., and López-Valenzuela, J.A. (2010). Changes in protein expression associated with chilling injury in tomato fruit. J. Am. Soc. Hortic. Sci. **135:** 83–89.

Vicente, A.R., Saladié, M., Rose, J.K.C., and Labavitch, J.M. (2007). The linkage between cell wall metabolism and the ripening-associated softening of fruits: Looking to the future. J. Sci. Food Agric. **87:** 1435–1448.

Vrebalov, J., Pan, I.L., Arroyo, A.J.M., McQuinn, R., Chung, M., Poole, M., Rose, J.K.C., Seymour, G., Grandillo, S., Giovannoni, J., and Irish, V.F. (2009). Fleshy fruit expansion and ripening are regulated by the tomato SHATTERPROOF gene TAGL1. Plant Cell **21:** 3041–3062.

Wang, H., Schauer, N., Usadel, B., Frasse, P., Zouine, M., Hernould, M., Latché, A., Pech, J.C., Fernie, A.R., and Bouzayen, M. (2009). Regulatory features underlying pollination-dependent and -independent tomato fruit set revealed by transcript and primary metabolite profiling. Plant Cell **21:** 1428–1452.

Weigelt, K., Küster, H., Radchuk, R., Müller, M., Weichert, H., Fait, A., Fernie, A.R., Saalbach, I., and Weber, H. (2008). Increasing amino acid supply in pea embryos reveals specific interactions of N and C metabolism, and highlights the importance of mitochondrial metabolism. Plant J. **55:** 909–926.

Yano, K., Watanabe, M., Yamamoto, N., Tsugane, T., Aoki, K., Sakurai, N., and Shibata, D. (2006). MiBASE: A database of a miniature tomato cultivar Micro-Tom. Plant Biotechnol. **23:** 195–198.

Yeats, T.H., Howe, K.J., Matas, A.J., Buda, G.J., Thannhauser, T.W., and Rose, J.K. (2010). Mining the surface proteome of tomato (*Solanum lycopersicum*) fruit for proteins associated with cuticle biogenesis. J. Exp. Bot. **61:** 3759–3771.

Zhang, L.L., Chen, K.S., and Xu, C.J. (2008). Identification and characterization of transcripts differentially expressed in peel and juice vesicles of immature and ripe orange (*Citrus sinensis*) fruit. Plant Mol. Biol. Rep. **26:** 121–132.

Zhang, Y., Sun, K., Sandoval, F.J., Santiago, K., and Roje, S. (2010). One-carbon metabolism in plants: Characterization of a plastid serine hydroxymethyltransferase. Biochem. J. **430:** 97–105.

This information is current as of March 23, 2012